Lung and Lung Lobe Segmentation Methods by Fraunhofer MEVIS

Bianca Lassen, Jan-Martin Kuhnigk,
Michael Schmidt, and Heinz-Otto Peitgen

Fraunhofer MEVIS,
Universitaetsallee 29, 28359 Bremen, Germany
http://www.mevis.fraunhofer.de

Abstract. In this paper we present one method for segmenting the lungs
and three methods to segment pulmonary lobes from thoracic CT im-
ages. The lung segmentation procedure is fully automated and uses a
sequence of morphological operations to refine an initial threshold-based
segmentation of the pulmonary airspaces. Based on its results, lobe seg-
mentation is performed. The three presented lobe segmentation methods
differ substantially in grade of automation. The first method is a fully
automatic segmentation algorithm based on a watershed transformation.
The pulmonary fissures, the bronchial tree, and the vessels are segmented
to provide the input information for the watershed transformation. The
second presented method is based on a precalculated lobe segmentation
and offers an interactive correction of the given segmentation. The user
can iteratively modify a lobar boundary by drawing its correct course
onto regions of insufficient segmentation. The instant feedback allows
the user to check the result and to continue correction until the seg-
mentation result is satisfying. The third segmentation algorithm is an
interactive method working completely from scratch that requires only a
lung mask as input. Analogous to the second method the user draws the
fissure on several slices and gets immediate feedback that allows further
interaction until the segmentation result is adequate.

1 Introduction

We present one fully automatic lung segmentation method and three lung lobe
segmentation approaches that differ in their grade of automation:

1. Automatic Lung Lobe Segmentation [1][2]
2. Automatic Lung Lobe Segmentation with Interactive Correction [3]
3. Interactive Lung Lobe Segmentation from Scratch [3]

These three lung lobe segmentation methods are presented in a single paper
for two reasons. First, they complement each other and we use them in a way
that requires minimal interaction time. A lung data set is at first processed us-
ing the fully automatic segmentation algorithm. If the result is satisfactory no
further steps and no interaction at all are needed. In case of local inaccuracies
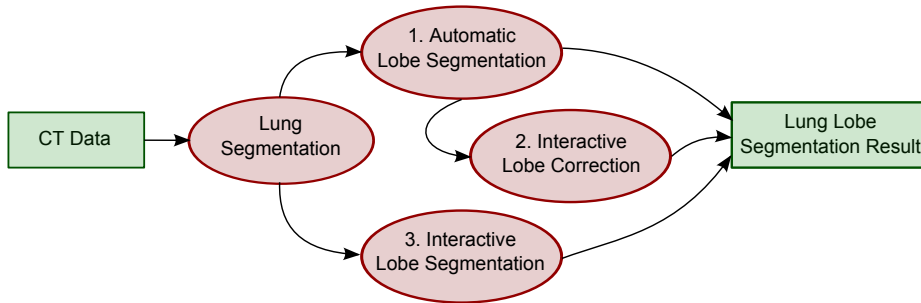
Fig. 1: Relation of the presented lung segmentation and the three lung lobe segmentation methods.

the user can improve the segmentation with the presented correction method. If for reasons such as severe pathologies or low resolution data the automatic lobe segmentation completely failed the user can segment the lobes from scratch using the third presented method. This combination of the algorithms (see Figure 1) shall ensure that a satsifactory lobe segmentation is possible for each and every pulmonary CT dataset. Second, the three segmentation methods are all based on the same lung segmentation algorithm. In the following, the commonly used lung segmentation algorithm as well as the three lobe segmentation algorithms are describes in more detail. All presented methods are implemented in the development environment for medical image processing and visualization MeVisLab [4].

2 Automatic Lung Segmentation

The basic lung segmentation method used in the challenge was described in detail in [1] and [5]. Briefly, the method starts with a low-resolution (voxel size $2 \times 2 \times 3$ mm) analysis of the CT data to first locate and then coarsely segment the pulmonary airspace with a fixed-threshold region growing. Using the low-resolution lung mask, an approximate lung bounding box is extracted and an appropriate lung segmentation threshold is computed by histogram analysis. Based on this information, the pulmonary airspace is segmented in the full resolution image using a threshold-based 3D region growing (Figure 2b). For separation of the left and right lung area a coarse airway segmentation is performed (Figure 2c). A 2D shape and size analysis is performed on the low-resolution mask to find trachea candidates, which are then grouped in 3D to identify the most likely trachea candidate. After prefiltering the original CT data using the output of minimum and maximum kernel filters (kernel size 5x5x5) at equal weight, an adaptive threshold-based 3D region growing is used to segment at least the trachea and main stem bronchi. After the segmentation, a morphological leak removal step is applied to detect and possibly remove large airway mask leaks that could disturb lung segmentation. For lung separation and mask closing, the

original data is first downsampled trilinearly to isotropic 1.5 mm voxels to speed up processing and reduce image noise. Using the dilated airway mask to block passage through the main stem bronchi, the left and right lung are separated using a 3D watershed segmentation (Figure 2d). Subsequently, a morphological closing step is performed to include larger pulmonary blood vessels and high-density lung pathologies (Figure 2e). This is done by applying a 3D rolling ball algorithm. A first application uses a 13 mm radius to close major interior holes, resulting in a *pre-closed mask*. In a second closing step, another rolling ball algorithm with a 5 mm radius is applied to the union of the unclosed mask and the core of the pre-closed mask (defined as the regions being further away than 5 mm from its boundaries). In order to obtain highly accurate lung boundaries after upsampling to the original resolution, the lung boundaries are refined using the high-resolution airspace mask.

3   Automatic Lung Lobe Segmentation

The basic idea of the presented automatic lung lobe segmentation method is the combination of several features to avoid a strong dependency of the existence and visibility of pulmonary fissures. We combine the information of fissures, the pulmonary vessels and the bronchial tree into a single cost image that is used for a watershed transformation. In the following the segmentation and processing of the particular structures and the generation of markers for each of the lobes is described.

3.1   Pulmonary vasculature

Due to the high contrast between blood vessels and lung parenchyma a 3D region growing algorithm can perform a coarse segmentation of the pulmonary blood vessels (see Figure 4b). The seed points for this procedure are found automatically by locating a high density area in the region where the hilus is expected. On the assumption that there are few larger vessels close to the lobe boundaries, a Euclidean distance transformation from each voxel inside the lung region to the closest vessel voxel is calculated. The result distance transformation image shows high intensity values at the lobar boundaries (see Figure 4e).

3.2   Bronchial tree

The airway lumen is separated from the parenchymal tissue with similar CT density mainly by thin airway wall structures, making its segmentation challenging due to partial volume effects and image noise. We apply two preprocessing steps to mitigate these problems. First, a Gaussian smoothing with fixed kernel width ($\sigma = 0.75\,mm$) is applied to the image although the blurring increases the partial volume related problems. Then, a bronchi enhancement filter is used to remove influence of partial volume effects and Gaussian blurring on the airway lumen. For each voxel, this filter casts 26 star-shaped rays into the neighbourhood and

a. Chest dataset:
Unsegmented CT data.

b. Airspace Segmentation:
Airspace extraction by
fixed-threshold region
growing.

c. Bronchi Segmentation:
Optimal threshold region
growing using seeds derived
from the airspace mask **b**.

d. Lung Separation:
Subdivision of the remaining
airspaces into left and right
parenchyma regions.

e. Lung Closing:
Inclusion of the pulmonary
blood vessels previously
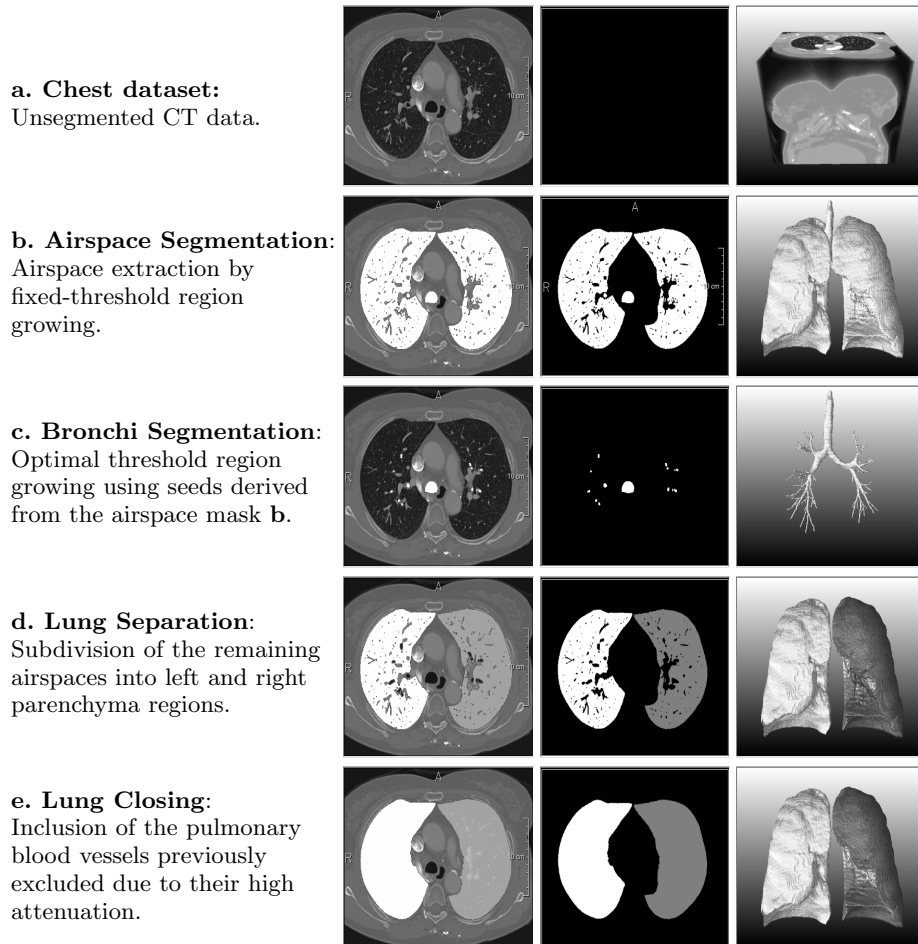excluded due to their high
attenuation.

Fig. 2: The essential processing steps of the automated lung segmentation procedure visualized on a single slice overlaying the original data (left), isolated (center), and as 3D volume rendering (right).

analyzes voxel values along the rays, grouped by all of the 9 main cut planes passing through the voxel. If the voxel is surrounded by bright voxels in at least three of the cut planes, an amount relative to the brightness of the surrounding structure is removed from the central voxels intensity.

After this preprocessing, a 3D region growing algorithm can be used to extract the airway lumen from the CT scan. The region growing is initialized with the result of the coarse airway segmentation used in the automatic lung segmentation (see Sec. 3) and region growing is executed iteratively with increasing thresholds until a critical raise in the segmented volume is detected, indicating leakage into the parenchymal tissue. Furthermore, the same leak removal as in Section 2 is applied, this time with a higher sensitivity to remove also smaller

leaks that could impair airway analysis required for lobar cone computation (Figure 5). As for the pulmonary vasculature, a Euclidean distance transformation is calculated to receive high intensities at the lobar boundaries.

3.3 Pulmonary fissures

The pulmonary fissures are often only incompletely or not clearly visible in CT data because of severe lung diseases, low image resolution, or absence of a fissure. However, in regions of a visible fissure this information is beneficial for a precise lobe segmentation. A common method to enhance characteristic structures is a feature analysis of the Hessian matrix.

Considering the Eigenvalues $|\lambda_1| \leq |\lambda_2| \leq |\lambda_3|$ of the Hessian matrix fissures can locally be modeled as sheets. Voxels belonging to the fissure have one large negative Eigenvalue that results from the large intensity gradient orthogonal to the fissure plane and two small Eigenvalues that reflect the homogeneity along the fissure: $|\lambda_1| \approx |\lambda_2| \approx 0$ and $\lambda_3 \ll 0$. Based on these characteristic features a fissure enhancement can be calculated.

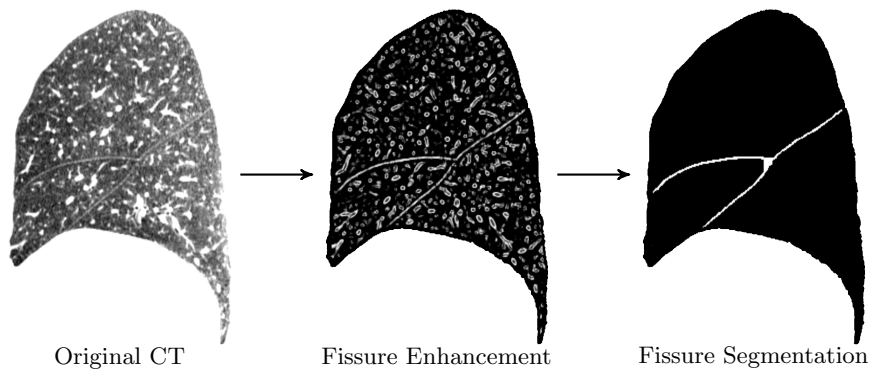| Original CT | Fissure Enhancement | Fissure Segmentation |

Fig. 3: A sagittal CT image with fissure enhancement and fissure segmentation after a vector-based connected component analysis.

In the next step a 3D vector-based connected component analysis (closely related to the approach by Rikxoort et al. [6]) is performed on a voxel set of fissure candidates estimated by the fissure enhancement. Since the curvature of fissures is locally low neighboring fissure voxels have a similar direction of the largest eigenvector. All adjacent voxels with an absolute inner product of the largest normalized eigenvectors ≥ 0.98 are clustered to a connected component. Components ≥ 0.1ml are kept and small gaps are closed by a morphological closing. Figure 3 shows an example of fissure enhancement and following fissure segmentation. To introduce the fissure information into the cost image a Euclidean distance transformation is calculated in a distance of 2 cm around the
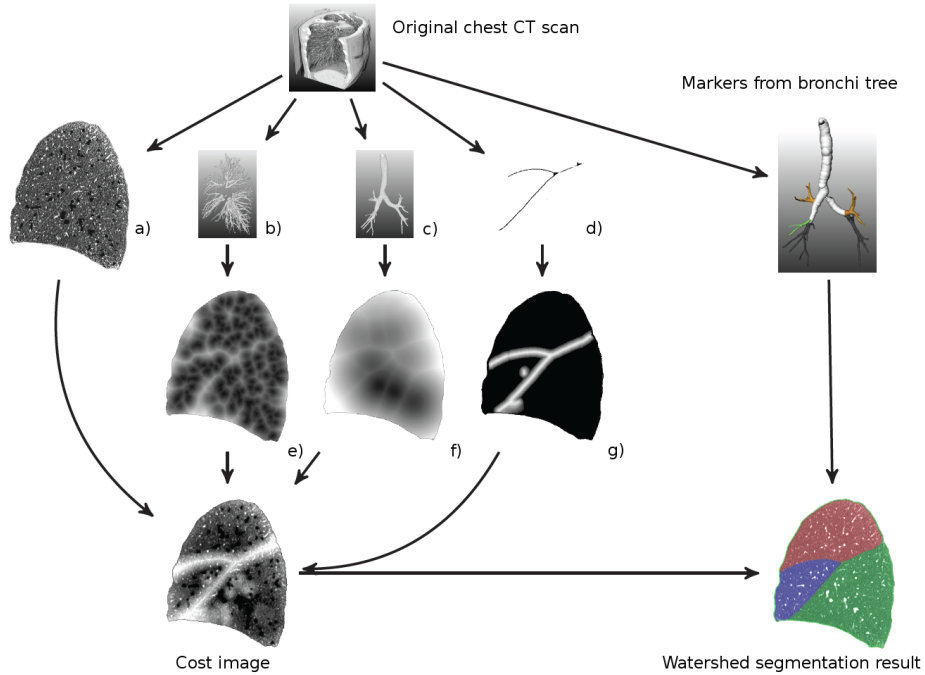
Fig. 4: Schematic diagram of the automatic lobe segmentation algorithm. From the original chest CT scan four features are extracted to calculate the cost image for the watershed transformation: a) the original data with the blood vessels masked out b) the pulmonary vasculature c) the bronchial tree and d) the pulmonary fissures. A distance transformation is calculated from e) the vasculature, f) the bronchial tree and g) the fissures (inverted) to get high intensity values at the lobar boundaries. All four inputs are equally weighted to obtain the cost image for the watershed transform. Markers for the lobes are calculated automatically from the bronchial tree.

fissures. The result is inverted and the square is calculated to get high values at the fissures (see Figure 4g).

3.4 Lobe marker generation

Nicely reflecting the lung lobes in its branching structure, the bronchial tree (3.2) suggests itself as a source of lobe markers for the watershed segmentation used in our automatic lobe segmentation.

First, we generate a directed, acyclic graph representing the bronchial tree structure by applying a thinning algorithm [7] to the bronchial tree segmentation. The nodes of this graph represent branching points of the bronchi whereas each edge represents the centerline of a bronchus section between two consecutive
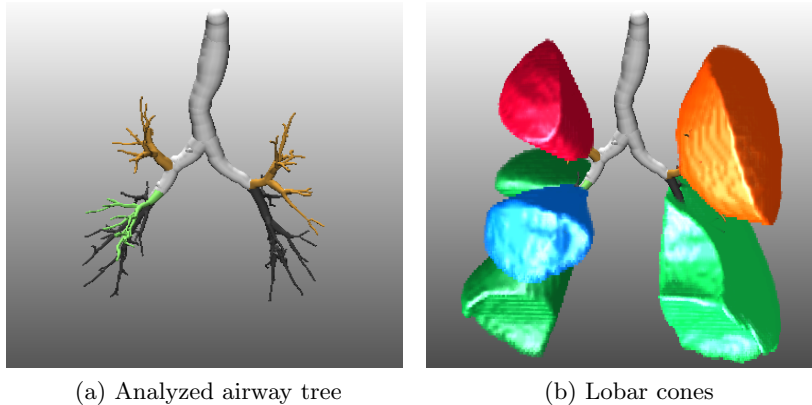
(a) Analyzed airway tree (b) Lobar cones

Fig. 5: Result of the advanced bronchi segmentation after lobar bronchi analysis (a) and the resulting lobar cones (b) that are used for lobe marker generation.

branching points and is directed from its proximal to the distal point. For each edge in this graph, we calculate the subtree mask volume and its center of gravity. We then separate the graph into pairs of disjoint subtrees representing different anatomical units (left and right lungs, upper and middle/ lower lobes, middle and lower lobe) by iteratively searching for sibling edges with maximally large and well separated subtrees. The subtree separation score is calculated as the squared distance of both subtrees' centers of gravity along an appropriate separation axis, multiplied by the smaller subtrees mask volume.

In contrast to previous publications, where markers were directly computed from the lobar bronchi (Figure 5a), we now additionally compute lobar cones extending until the lung borders based on each lobe's root node and a PCA of the terminal nodes (Figure 5b). This increases segmentation accuracy when only few or no distal bronchi were detected by the bronchial tree segmentation for one or more lobes. Wherever cones of different lobes intersect they are cropped with an additional safety margin.

3.5 Marker-based watershed transformation

The four calculated feature images based on the bronchial tree, vessels, fissures, and original image with vessels masked out are combined with equal weight to a cost image. The original image is regarded to enhance the fissures that are possibly not found by the fissure segmentation method due to pathological thick fissures and corresponding high intensity values.

The 3D watershed transformation is performed to segment the lung lobes based on the cost image and the lobe markers. Figure 4 shows all four inputs of the cost image with the resulting final cost image and the lung lobe segmentation. The method was evaluated on 42 CT data sets against a reference segmentation manually segmented by a human expert. For details see [2].

4 Interactive Lung Lobe Correction

The interactive correction method offers intuitive correction of inadequate lung lobe segmentations. Besides an existing lobe segmentation, no further input is needed. Thus, the correction can be applied to segmentations from arbitrary origin and modality. The processing of the fissures occurs successively: right major fissure, right minor fissure, and left major fissure. When regarding the right minor fissure only the upper and middle lobe are visible to avoid intersection with the major fissure. The user can simply skip a fissure if no changes are needed.

To correct an existing segmentation, the user simply traces the lobar boundary on a slice of arbitrary orientation. The fissure is immediately adapted on the current slice and on neighboring slices. Thus the user gets a fast feedback and can continue correcting until the result is satisfying. The crucial point is to define the 3D influence range of such a 2D user interaction. Therefore, the depth of the 3D influence region depends highly on the amount of difference between initial and corrected boundary in the current plane. In the following, initializing with a given existing segmentation and the handling of user input are described.

4.1 Initialization with a given segmentation

In order to import a given segmentation a rank-based boundary filter is applied to find the requested fissure. The filter is limited to the boundaries inside the lung and to the appropriate lobes to distinguish between major and minor fissure. All voxels under a 3x3x1 kernel are sorted in ascending manner and the result value is the index of the position of the current voxel. In the next step a thresholding thins out the fissure surface to get only voxel of high curvature and only the voxels on each forth axial slice are regarded. The resulting subset of fissure voxels is converted to a set of 3D sampling points (see Figure 6). From these sampling points the center of gravity and the orientated bounding box are calculated. Based on this spatial orientation a regular mesh is generated and the sampling points are projected onto the mesh. To adapt the mesh to the fissure, the grid points of the mesh are translated according to the offset between the closest projected sampling point and its original location. A smoothing follows to decrease irregular distances between the grid points. The adapted mesh represents the fissure surface that can be modified by the user.

4.2 Processing of user interaction

Each curve drawn by a user is also converted to a set of sampling points and added to the set of fissure sampling points. Before recalculating a new fissure surface based on the updated set of sampling points the source of inaccurate segmentation must be eliminated. Thus these sampling points that represent a leakage must be deleted from the set of fissure sampling points. In order to find these points a 3D region around the user curve is defined and all points inside this region are removed. The region is calculated by several morphological operations in 2D and extrapolated to 3D. The extent of the region mainly depends on the

(a) Fissure (yellow curve) before correction.

(b) 3D rendering of the surface sampling points before interactive correction.

(c) Manually sketched user curve (red curve) and fissure (yellow curve) after correction.

(d) 3D rendering of the surface sampling points after interactive correction.
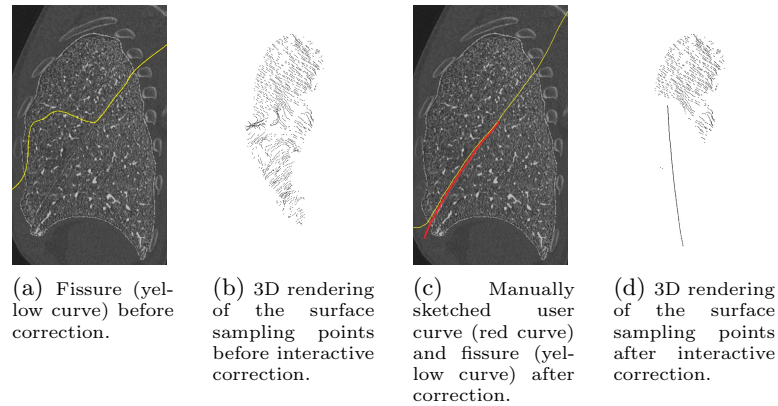
Fig. 6: Interactive correction of a pulmonary fissure in sagittal view. The user interaction leads to a thinning of the original sampling points.

distance between the user drawn curve and the original fissure on the interaction slice. A significant correction on a slice leads to a larger 3D impact region than a minor correction. The key issue is to find a balance between removing as many as possible sampling points that are responsible for a inaccurate segmentation while keeping as many as possible appropriate sampling points.

When the user has finished correction the fissure surface is used to split the lung mask into two parts. The resulting lobe candidates are classified by a simple heuristic based on the center of gravity. The upper lobe is expected to have the highest z-coordinate followed by the middle and lower lobe. The method was evaluated on 3 CT scans with a reference standard provided by an expert. Figure 7 shows an example of an interactive correction of a given segmentation with a strong leakage. For details see [3].

5 Interactive Lung Lobe Segmentation from Scratch

The interactive lung lobe segmentation approach from scratch is meant for cases without an automatic lobe segmentation result. It only requires a lung mask as input. The method is based on the same approach as the interactive lung lobe correction (see Chapter 4) except that no sampling points have to be deleted because there is no given segmentation. The user sketches the pulmonary fissure on several slices in arbitrary orientation (see Figure 8). Analogous to the correction approach the curves are converted to a set of sampling points which are used to calculate a fissure surface that extends the whole lung. Any user curve results in an immediate recalculation of the fissure surface. Thus the user can again sketch the fissure on any more slices until the segmentation result is adequate. Since the fissure always extends over the total lung the lobes can easily be estimated by separating the lung by the fissure surface. Empirical studies shows that best segmentation results are achieved by sketching the fissure in sagittal orientation.
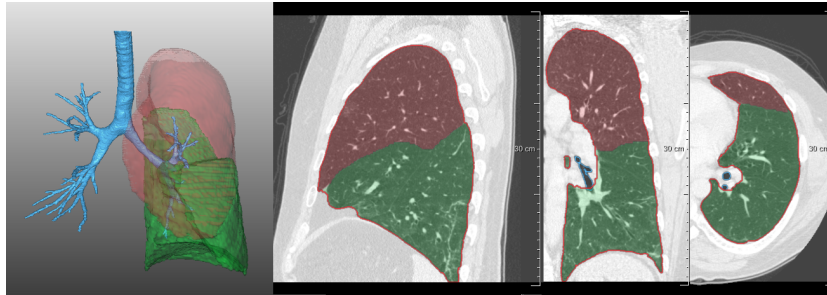
(a) Lung lobe segmentation before correction.
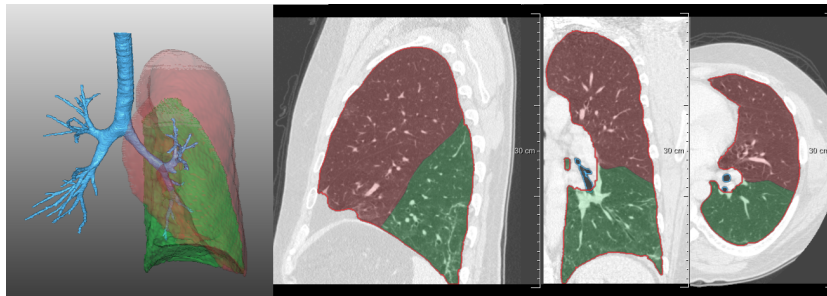
(b) Lung lobe segmentation after correction.

Fig. 7: Correction of a lobe segmentation of a left lung. The automatic segmentation result (a) shows a strong leakage that can be correction by two interactively sketched curves.

The interactive lung lobe segmentation approach was evaluated on 25 CT data sets. For details see [3].

6 Experiments and Results

6.1 Experiment Setup

All algorithms were implemented using the in-house version of the rapid prototyping and development platform MeVisLab [4]. First, the automated lung segmentation was applied to the data. Based on the lung segmentation results, both automatic (method 1) and interactive (method 3) lobe segmentations were performed. The results of the automatic lobe segmentation (method 1) were then additionally corrected using the interactive correction (method 2). Where correction did not make sense because of a totally failed automatic segmentation, it was possible to delete all prior results and start from scratch, which is equivalent to using method 3.

To support the interactive procedures (lobe segmentation methods 2 and 3), a dedicated MeVisLab GUI application was developed. Both the interactive seg-

(a) Four sagittal fissure curves (dark red), manually sketched in 2D by an observer.

(b) Fissure curves (dark red), visualized using semi-transparent 3D surface renderings of the lungs in slanted coronal view.

(c) Calculated fissure surface (grey) that divides the left lung into upper and lower lobe.

(d) Calculated left major fissure surface (dark red) visualized using semi-transparent 3D surface renderings of the lungs in slanted coronal view.
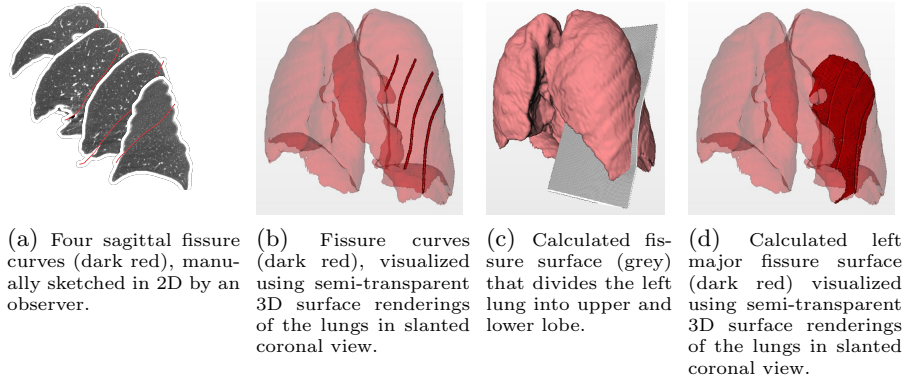
Fig. 8: From scratch segmentation of a left lung with four manually sketched fissure curves.

mentation and correction were performed by an experienced lung image analyst after a few hours of training using mostly sagittal views on the data.

6.2   Segmentation Accuracy

The overlap scores in comparison with the LOLA11 reference standard are given in Tables 1 to 4.

Table 1: Overlap scores for the Automated Lung Segmentation for the 55 scans in LOLA11.

	mean	SD	min	Q1	med.	Q3	max
left lung	0.974	0.098	0.277	0.987	0.992	0.995	0.999
right lung	0.972	0.135	0.000	0.991	0.994	0.996	0.999
score	**0.973**						

6.3   Time Consumption

For processing of the test data, a two year-old standard quad-core Windows PC with 8 GB of RAM was used.

Processing times for the methods were as follows (preprocessing time for lung segmentation is not included for the lobe segmentation methods):

(*) **Automatic Lung segmentation required about 1 minute** per case on average. Times ranged between 0.5 and 3 minutes and depended on data size, and on whether airway leaks were detected and removed or not.

Table 2: Overlap scores for the Automatic Lobe Segmentation (method 1) for the 55 scans in LOLA11.

	mean	SD	min	Q1	median	Q3	max
left upper lobe	0.922	0.163	0.198	0.94	0.978	0.991	0.997
left lower lobe	0.885	0.229	0.000	0.939	0.964	0.983	0.996
right upper lobe	0.921	0.088	0.604	0.897	0.960	0.978	0.998
right middle lobe	0.765	0.299	0.000	0.773	0.886	0.945	0.989
right lower lobe	0.914	0.176	0.000	0.936	0.968	0.983	0.998
score	**0.881**						

Table 3: Overlap scores of the Interactive Lobe Segmentation Correction (method 2) applied to the automatically generated results (c.f. Table 2) for the 55 scans in LOLA11.

	mean	SD	min	Q1	median	Q3	max
left upper lobe	0.947	0.132	0.203	0.968	0.984	0.991	0.996
left lower lobe	0.911	0.210	0.000	0.954	0.978	0.983	0.997
right upper lobe	0.937	0.079	0.675	0.935	0.969	0.982	0.995
right middle lobe	0.837	0.235	0.000	0.829	0.923	0.961	0.987
right lower lobe	0.960	0.070	0.541	0.955	0.977	0.988	0.999
score	**0.918**						

Table 4: Overlap scores for the Interactive Lobe Segmentation (method 3) for the 55 scans in LOLA11.

	mean	SD	min	Q1	median	Q3	max
left upper lobe	0.945	0.141	0.207	0.964	0.985	0.99	0.996
left lower lobe	0.913	0.212	0.000	0.962	0.979	0.984	0.994
right upper lobe	0.943	0.079	0.678	0.946	0.974	0.987	0.995
right middle lobe	0.850	0.224	0.000	0.861	0.932	0.963	0.990
right lower lobe	0.962	0.071	0.542	0.968	0.979	0.987	0.997
score	**0.923**						

(1) **Automatic Lobe segmentation required about 9 minutes** per case on average. Times ranged between 2 and 31 minutes, growing with data size and the depth of the segmented airway tree.

(2) **Interactive lobe correction required 1.5 minutes of interaction** per case on average. Times ranged between 0 and 3 minutes. In addition, 1 minute of pre- and post-processing time needs to be spent, but only for those cases where the existing segmentation was insufficient. Individual averages for each fissure (left major, right major, right minor) were 23, 32, and 32 seconds, respectively.

(3) **Interactive lobe segmentation required about 4 minutes of interaction** per case on average. Times ranged between 2 and 7 minutes. In addition, about 1 minute per case was required for automatic pre- and postprocess-

ing. Individual averages for each fissure (left major, right major, right minor) were 78, 84, and 62 seconds, respectively. In a previously published study (see [3] for details) interaction time was slightly smaller. The increase observed for this study could be due to the higher ratio of pathological lungs.

In summary, it takes about 10 minutes to segment lungs and lung lobes from a typical chest CT dataset using the presented fully-automated methods. If results are to be interactively corrected, this takes about 2 minutes in addition. To segment only the lungs automatically and then segment the lung lobes interactively, the whole process takes about 6 minutes per case.

6.4 Amount of Interaction

For the interactive methods, the number of interactions was measured. Besides actual fissure drawings, 'undo' and 'undo all' counted as interactions.

(1) **Interactive lobe correction required 7 interactions** per case on average. The number of interactions ranged between 0 and 18. For each individual fissure (left major, right major, right minor), the average number of interactions was 2, 3, and 3, respectively.
(2) **Interactive lobe segmentation required 20 interactions** per case on average. The number of interactions ranged between 8 and 30, subjectively increasing with fissure irregularity and incompleteness. For each individual fissure (left major, right major, right minor), the average interaction counts were 6, 7, and 6, respectively.

7 Discussion

7.1 Evaluation results

The accuracy of the lobe segmentation results correlates with the amount of interaction. Method 3 shows best results but requires the largest amount of interaction whereas method 1 got the lowest score compared to the other methods with no interaction at all. Method 2 turns out to be the best trade-off between accuracy and interaction. Only little interaction is required to obtain almost as accurate results as method 3.

The largest variations compared to the reference occurred in the right middle lobe for all three methods. The middle lobe is usually smaller than the other lobes thus inaccuracies have a stronger impact on the overlap error. Moreover, the minor fissure which delimits the middle lobe from the upper lobe is more often incompletely or not clearly visible than the major fissures.

7.2 Limitations

The limitations of the lung segmentation are mainly due to its basic approach of iterative refinement of an initial, purely connectivity and threshold-based

airspace segmentation. Whenever a pulmonary high-density pathology such as a large tumor or atelectasis is connected to the lung boundaries, it will not be covered by the lung mask unless it is small enough to be included by the rolling ball closing. Another problem is occasional leakage of the airspace segmentation into extrapulmonary airspaces such as the colon or esophagus. Lastly, while lung separation was shown to be very robust also for very inflated lungs [5], cases where one lung is very small or missing entirely cannot currently be detected and will most likely be segmented incorrectly. Regarding the acquisition parameters (e.g. reconstruction increment and kernel, dosage, inspirations state), the lung segmentation algorithm has no special requirements.

All three presented lobe segmentation methods require a lung segmentation as input but are not limited to certain types of scans or exclude pathological lungs in general. Nevertheless, some pathological lungs can lead to problems for the automatic segmentation (method 1). Especially occluded bronchi can preclude a proper bronchi segmentation, which is required for the generation of classification lobe markers for the watershed transform. Moreover, due to the very simplistic vessel segmentation included, high-density pathologies are often mistaken for vasculature and can lead to inaccuracies when located near the lobar boundaries. In particular, this includes thickened fissures.

The interactive correction and segmentation approaches (methods 2 and 3) do not require image features and are therefore not limited to CT data. One limitation of the interactive methods is accuracy. Since the underlying fissure surface is inter- or extrapolated for most slices, the segmentation result might not be voxel-accurate at the lobar boundaries. Even in regions with an interactively sketched curve the fissure surface might minimally differ from this curve because of a global smoothing of the underlying mesh. Inaccuracies arise in particular at lobar boundaries with an extremely angular shape.

8   Summary and Conclusion

We have proposed one automatic lung segmentation method and three partly related lobe segmentation approaches. If preprocessing time is irrelevant the three proposed lung lobe segmentation approaches are best applied in the following way to restrict interaction time: First, the automatic lobe segmentation (method 1) is performed. Then, in case of unsatisfying segmentation results, the interactive correction method (method 2) is applied. If the automatic segmentation completely fails the user can perform an interactive segmentation from scratch (method 3). For most cases the automatic segmentation provides appropriate results while the interactive correction or segmentation guarantee to get appropriate results even for very difficult cases.

References

1. J.-M. Kuhnigk, V. Dicken, S. Zidowitz, L. Bornemann, B. Kuemmerlen, S. Krass, H.-O. Peitgen, S. Yuval, H.-H. Jend, W. S. Rau, and T. Achenbach. New tools

for computer assistance in thoracic CT – part I: Functional analysis of lungs, lung lobes, and bronchopulmonary segments. *RadioGraphics*, 25(2):525–536, 2005.

2. Bianca Lassen, Jan-Martin Kuhnigk, Ola Friman, Stefan Krass, and Heinz-Otto Peitgen. Automatic segmentation of lung lobes in CT images based on fissures, vessels, and bronchi. In *ISBI*, pages 560–563, 2010.

3. Bianca Lassen, Jan-Martin Kuhnigk, Eva M. van Rikxoort, and Heinz-Otto Peitgen. Interactive lung lobe segmentation and correction in tomographic images. In *SPIE Med Imaging*, volume 7963, 2011.

4. MeVisLab. Medical image processing and visualization (v2.3). 2011. URL: www.mevislab.de.

5. Jan-Martin Kuhnigk. *Quantitative Analysis of Lung Morphology and Function in Computed Tomographic Images*. PhD thesis, 2008. URL: http://nbn-resolving.de/urn:nbn:de:gbv:46-diss000110480.

6. E. M. van Rikxoort, B. de Hoop, S. van de Vorst, M. Prokop, and B. van Ginneken. Automatic segmentation of pulmonary segments from volumetric chest CT scans. *IEEE Trans Med Imaging*, 28(4):621–630, 2009.

7. D. Selle, B. Preim, A. Schenk, and H.-O. Peitgen. Analysis of vasculature for liver surgical planning. *IEEE Transactions on Medical Imaging*, 21(11):1344–1357, 2002.